Rostislav Kawulok, Lukáš Pindor, Radek Cieslar, Milan Plevko

Effect of the Strain Rate on (D)CCT Transformation Diagrams of Steel 25CrMo4

Abstract: The transformation kinetics during cooling of steels is most often documented in CCT and DCCT transformation diagrams, in cases where austenite was deformed prior to cooling. In such cases, attention is paid to austenite transformations in steel 25CrMo4. Within the research work, one CCT diagram and two DCCT diagrams with different strain rates (1 and 20 s^{-1}) were developed based on dilatometric tests and combined with metallographic analyses and hardness measurements. The work also involved the verification of the deformation effect shifting the onset of ferritic and pearlitic transformation to the left, i.e. towards higher cooling rates as well as the investigation of the effect of two strain rates. It was found that, compared to the lower strain rate (1 s^{-1}), the larger austenitic grain size combined with the higher strain rate (20 s^{-1}) delayed the transformation of ferrite and bainite. The above-named effect was explained by insufficient time for the full dynamic recrystallization process to take place during austenite deformation.

Key words: strain rate, transformation (D)CCT diagrams, austenite grain size

DOI: 10.32730/mswt.2024.68.4.2

1. Introduction

The knowledge of transformation temperatures is of great importance in terms of plastic deformation, particularly as regards the control of structural development, but in relation to the energy-power parameters of individual devices as well as the ductility of steels [1–3].

The transformation kinetics of steel depends on many factors, particularly on the chemical composition of the steel. During the cooling of a particular steel grade, the transformation kinetics of austenite is primarily a function of the cooling rate and the initial state of austenite. The initial state of austenite is defined by the homogeneity and size of individual grains. The initial austenite grain can be influenced by thermomechanical factors (temperature of austenitisation, holding time at the austenitisation temperature, the value of deformation, strain rate, etc.) [1–4].

The heating temperature and the temperature of holding time mainly affect the grain size and, possibly, the degree of the dissolution of precipitates and, consequently, the stability of austenite. It is generally assumed that, due to increasing temperature, the austenite grain size increases and, as a result, the transformation temperatures of the diffusion products of austenitic transformation (ferrite and pearlite) decrease. Healing processes, in particular recrystallisation, which by its nature fundamentally affects the size of the austenitic structure, also play a major role [1, 3–7].

If the austenite transformation is preceded by plastic deformation, the free energy and the thermodynamic instability of austenite increase, accelerating the decomposition of austenite into stable phases under given thermodynamic conditions. In other words, the transformation of plastically deformed austenite to ferrite or pearlite is faster than that of austenite without previous deformation, (which is confirmed in a number of publications [2, 3, 8–10]). According to the authors of work [11], the acceleration effect is especially evident at the beginning of these transformations and increases along with increasing deformation. The deformation increases the amount of lattice failures, which supports the diffusion of all atoms in the solid solution and leads to faster nucleation and growth of new phase nuclei. The nucleation sites of ferrite are the corner sites of grain boundaries, deformation bands, certain dislocations and subgrain boundaries. The nuclei usually form at the corners and deformation bands. However, the formation of nuclei at corners and deformation bands is not sufficient for spontaneous nucleation. Therefore, the most effective sites for ferrite nucleation are austenitic grain boundaries and deformation bands. At lower temperatures and larger deformation, the rate of nucleation is significantly greater than that of grain growth, which is a critical presumption for the formation of fine ferritic grains [1, 11–13].

Regarding the effect of the strain rate on the transformation kinetics of subcooled austenite, it can be stated that the strain rate affects the transformation primarily through the austenite grain size. If austenite is deformed and dynamic recrystallization is initiated, the increasing strain rate is known to push the initiation of dynamic recrystallization towards higher deformation and also higher deformation resistance. The resulting austenitic grain size may be higher, particularly in relation to smaller deformation than necessary for the full progress of dynamic recrystallisation. Bigger austenite grain sizes lead to the slower transformation of austenite into ferrite and pearlite [14–16].

However, some studies imply that the combination of increased strain rate and higher temperatures increases the volume fraction of ferrite in the structure, whereas the fraction of ferrite in the structure decreases along with the decreasing strain rate and temperature [8, 17].

At higher strain rates (above 100 s^{-1}), adiabatic heating (heat of deformation) may influence the austenite grain size, which again could lead to dynamic recrystallization, as has already been predicted by Zener and Hollomon. Studies concerning the effect of the strain rate on TRIP the transformation-induced plasticity (TRIP) of steel revealed that the main effect of the strain rate is the adiabatic heating of the

Ing. Rostislav Kawulok, Ph.D.; Ing Lukáš Pindor, Ph.D.; Ing. Radek Cieslar; Ing. Milan Plevko – Třinecké železárny a.s.
Corresponding author: Rostislav.Kawulok@trz.cz; Lukas.Pindor@trz.cz

material, leading to dynamic recrystallization and suppressing the deformation-induced transformation of martensite. Therefore, the transformation of austenite into martensite occurs more easily at lower strain rates. In general, the increasing strain rate suppresses the effect of deformation itself on the kinetics of austenite transformation [18–20].

To describe the transformation kinetics of austenite, TTT (Time Temperature Transformation) and CCT (Continuous Cooling Transformation) diagrams are developed for specific steels, whereas DCCT (Deformation Continuous Cooling Transformation) diagrams are created in cases of previous deformation. Such diagrams are usually developed on the basis of dilatometric tests, thermal analyses or mathematical modelling [21, 22].

There are a number of studies concerned with the effect of chemical composition, strain rate and austenite grain size on the transformation kinetics of austenite. However, there are not many scientific reference publications addressing the effect of previous deformation on the transformation of steels at different strain rates [23–25].

This article discusses the effect of previous deformation [involving two different strain rates (1 and 20 s^{-1})] on the transformation kinetics of steel 25CrMo4 during cooling. To this end, CCT and DCCT-type transformation diagrams were developed based on dilatometric tests supported by metallographic analyses.

2. Experiment

Steel 25CrMo4 belongs to low carbon and medium alloy steels. At the same time, this steel is characterised by lower hardenability (for medium-loaded machine parts) and is weldable and suitable for the production of seamless tubes. After hardening, the steel reaches a hardness of approximately 48 HRC. In the treated state, it reaches medium tensile strengths and yield point values with relatively high toughness. It is not susceptible to tempering embrittlement. The chemical composition of the test steel is presented in Table 1.

The dilatometric experiments involved the making of simple cylindrical specimens having a diameter of 6 mm and a length of 86 mm (see Fig. 1). The investigated steel was in the as-formed state (prepared from segments having a diameter of 300 mm, cut off from rolled seamless tubes).

The dilatometric experiments were performed using an optical dilatometer module [model 39112: Scanning Non-Contact Optical Dilatometer and Extensometer System with Green LED Technology (Dynamic Systems Inc.)] of the Gleeble 3800 plastometer. The optical dilatometric module is based on cross-sectional measurements (radial components of strain) of specimens with a repeatability of ± 0.3 µm in relation to a frequency of 2400 Hz, with a maximum temperature of 1200 °C [21, 26]. A schematic diagram of the device is presented in Fig. 2.

The first stage involved the identification of temperatures A_{c1} and A_{c3} (A_{c1} – pearlite to austenite transformation temperature, A_{c3} – ferrite to austenite transformation temperature), representing transformation temperatures during heating. In the case under discussion, the heating of the specimen was performed at a rate of 5 °C/s to a temperature of 500 °C. Afterwards, the rate was slowed down to 10 °C/min (0.167 °C/s) (to identify the region of transformation). The result of the test is presented in Fig. 3.

Based on the previous experiment aimed to determine temperatures A_{c1} (767 °C) and A_{c3} (827 °C), the specimens

Table 1. Chemical composition of test steel 25CrMo4 steel (wt. %)

C	Mn	Si	No	Cr	Mo	P	S
0.31	0.52	0.29	0.08	1.04	0.221	0.016	0.008

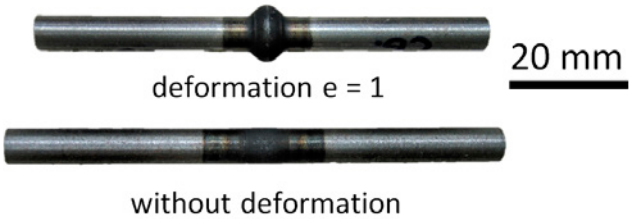

Fig. 1. Specimens used in the dilatometric tests; undeformed and after deformation e = 1

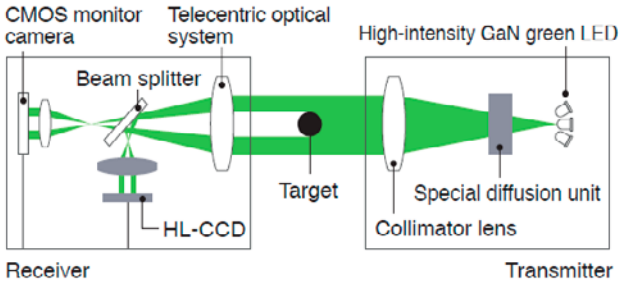

Fig. 2. Scanning Non-Contact Optical Dilatometer and Extensometer System with Green LED Technology (Dynamic Systems Inc.) of the Gleeble 3800 plastometer [21, 26]

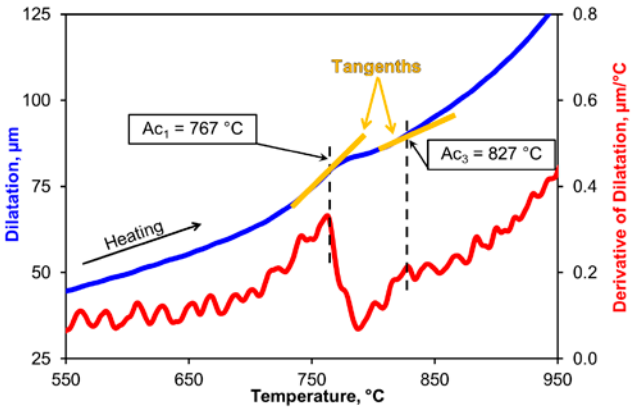

Fig. 3. Recording of temperature A_{c1} and A_{c3}

used in the development of (D)CCT diagrams were subjected to uniform austenitisation at a temperature of 870 °C and holding at the temperature for 5 minutes. In cases of the CCT diagrams, after holding at the temperature, the specimens were continuously cooled to room temperature at constant cooling rates restricted within the range of 0.2 °C/s to 50 °C/s. During the process, changes in the transverse expansion of the material were monitored and recorded. The completion of the development of the CCT diagram entailed the performance of another test (performed under the same temperature-time conditions as the previous tests, yet with a higher cooling rate of 100 °C/s). A specimen used in the above-named test had a special design (Fig. 4), i.e. hollow head sections enabling high-speed cooling performed using air jets. Regrettably, the special design of the specimens precluded the performance of deformation [27].

During the development of both variants of DCCT diagrams, the specimens were deformed by being subjected to uniaxial pressure, directly after being held at the austenitising temperature and prior to continuous cooling. The size of actual logarithmic deformation was e = 1 in both cases. The difference was the strain rate, i.e. 1 s^{-1} in relation to the first DCCT diagram and 20 s^{-1} in relation to the second DCCT diagram. As mentioned above, the element restricting the development of the DCCT diagrams was the maximum cooling rate of 50 °C/s (determined by the design of the specimens) [27]. Thus, in both cases of the DCCT diagrams, the cooling rates were restricted within the range of 0.2 °C/s to 50 °C/s.

The evaluation of measurement results was performed using semi-automatic CCT software, combining the tangential method and the derivative of the dilation curves to determine transformation temperatures (see Fig. 1). The results were then confronted with metallographic analyses (combination of optical metallography with QuickPHOTO INDUSTRIAL evaluation software) and hardness measurements (HV 30).

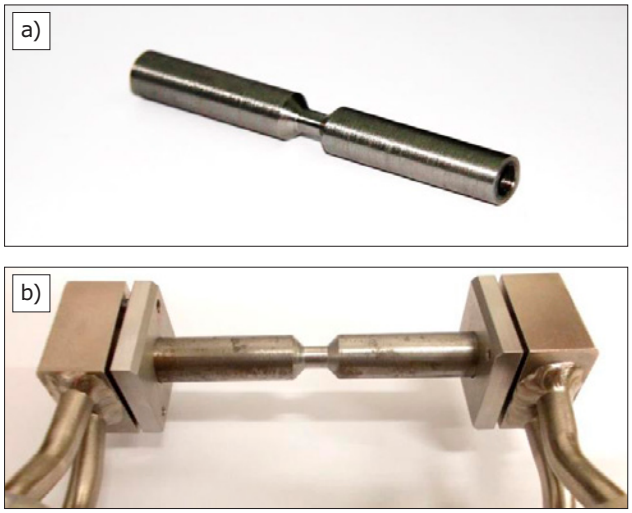

Fig. 4. Special specimen design for the dilatometric tests without deformation and higher cooling rates (100 °C/s) [27] a) specimen, b) specimen with cooling nozzles

3. Discussion

As mentioned above, because of its chemical composition, steel 25CrMo4 belongs to pro-eutectoid steel grades, where the presence of structural components such as ferrite, pearlite, bainite and martensite is expected in transformation diagrams. All three types of transformation diagrams were prepared based on the combination of dilatometric tests and metallographic analyses.

Figure 5 presents the CCT diagram of the steel, revealing the presence of all four austenite transformation products: the individual structural components bounded by the transformation rates. The transformation of austenite (A) into martensite (M) took place at cooling rates exceeding 2 °C/s, whereas bainite (B) formed in the steel at cooling rates

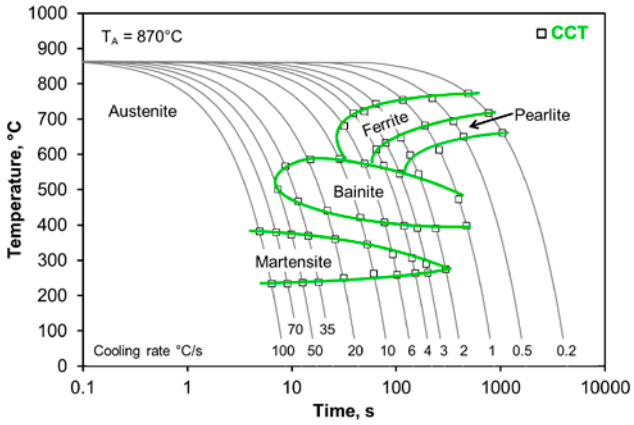

Fig. 5. Diagram (CCT) of steel 25CrMo4

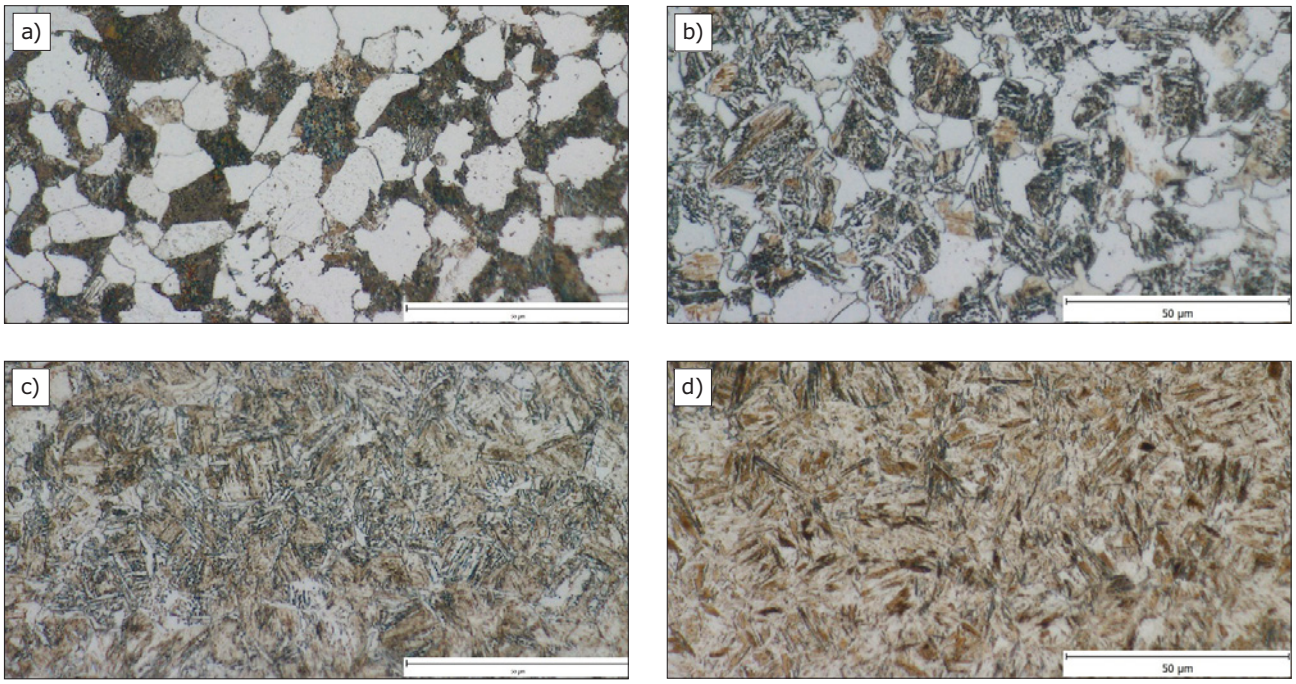

Fig. 6. Selected examples of metallographic analyses of CCT diagram samples:
a) 0,5 °C/s = 50 % F + 50 % P, b) 3 °C/s = 35 % F + 10 % P + 45 % B + 10 % M, c) 20 °C/s = 35 % B + 65 % M, d) 100 °C/s = 100 % M

restricted within the range of 1 °C/s to 50 °C/s. The diffusion products of ferrite (F) and pearlite (P) transformations are located in the diagram at cooling rates of 6 °C/s (F) and 4 °C/s (pearlite), respectively. The assumption that the martensitic region was continuously narrowed and closed along with the decreasing cooling rate was also confirmed [16].

The above-presented results were also confirmed through optical metallography. Selected specimens along with various cooling rates and corresponding structures (including the proportions of individual structural components) are presented in Fig. 6.

The DCCT transformation diagram constructed in relation to the size of actual deformation e = 1 and strain rate = 1 s^{-1} is presented in Fig. 7. Also in the aforesaid case (as expected), all four transformation products were represented. However, if compared to the previous CCT diagram, it was possible to observe slight shifts of some transformation regions. In particular, because of the previous deformation, it was possible to notice the significant acceleration in relation to the ferritic and pearlitic regions, starting to appear in the structure at a cooling rate of 20 °C/s (F) and that of 10 °C/s (P), respectively. The bainitic zone remained almost unchanged. The austenite to martensite transformation was slightly shifted towards lower temperatures. A slight shift was also observed in terms of the lowest cooling rate (bounded by 3 °C/s).

The results presented in the above diagram (Fig. 7) were verified using optical metallography (Fig. 8). Figure 8 presents the structures and fractions of the structural components of the deformed specimens (e = 1; $\dot{e}$ = 1 s^{-1}) cooled at a rate of 1 °C/s (a), 5 °C/s (b), 20 °C/s (c) and 50 °C/s (d). The comparison of the undeformed structure (Fig. 6) and the structure after deformation (Fig. 8) revealed that ferritic grains were slightly finer after deformation (which could indicate recrystallization).

Figure 9 presents the DCCT diagram of the test steel after deformation e=1 in relation to a strain rate of 20 s^{-1}. The pearlitic and martensitic transformations were not affected by the higher strain rate, with pearlite located at a rate of 10 °C/s and lower. Martensite was present in the structure at a rate of 3 °C/s and higher. However, the higher strain rate affected the transformation of austenite into ferrite and bainite. The ferritic transformation was limited by a maximum cooling rate of 14 °C/s. The area of bainite formation was restricted within the cooling rate range of 1.7 °C/s to 30 °C/s.

The dilatometric results were also confronted with the optical metallography results, which, including the

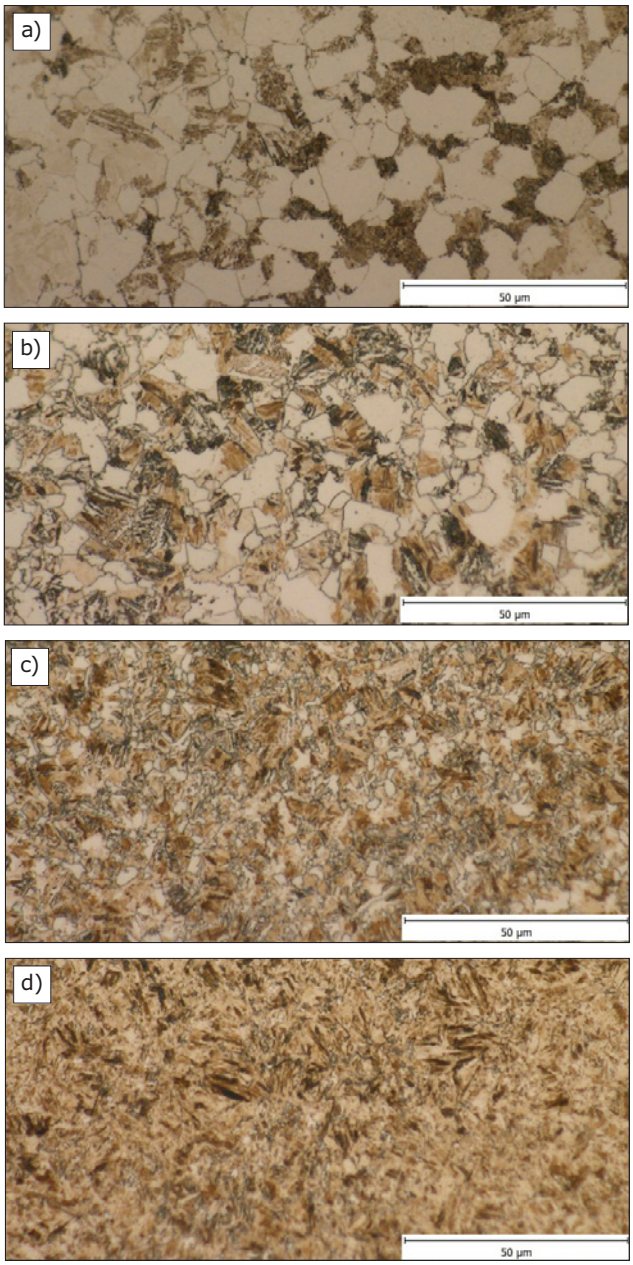

Fig. 8. Selected examples of metallographic analyses of samples from the DCCT diagram ($\dot{e}$ = 1 s^{-1}):
a) 1 °C/s = 60 % F + 40 % P
b) 5°C/s = 25 % F + 5 % P + 50 % B + 20 % M, c) 20 °C/s = 10 % F + 30 % B + 60 % M, d) 50 °C/s = 5 % B + 95 % M

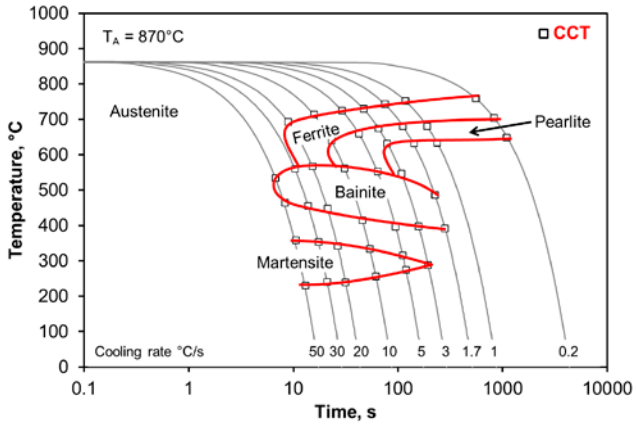

Fig. 7. Diagram (DCCT) of the 25CrMo4 steel with strain rate 1 s^{-1}

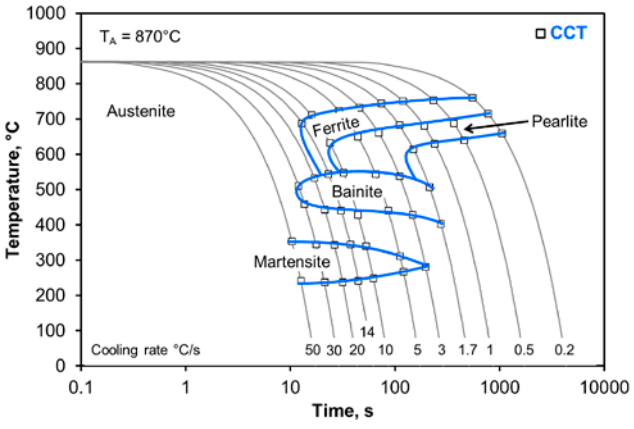

Fig. 9. Diagram (DCCT) of steel 25CrMo4 steel with strain rate 20 s^{-1}

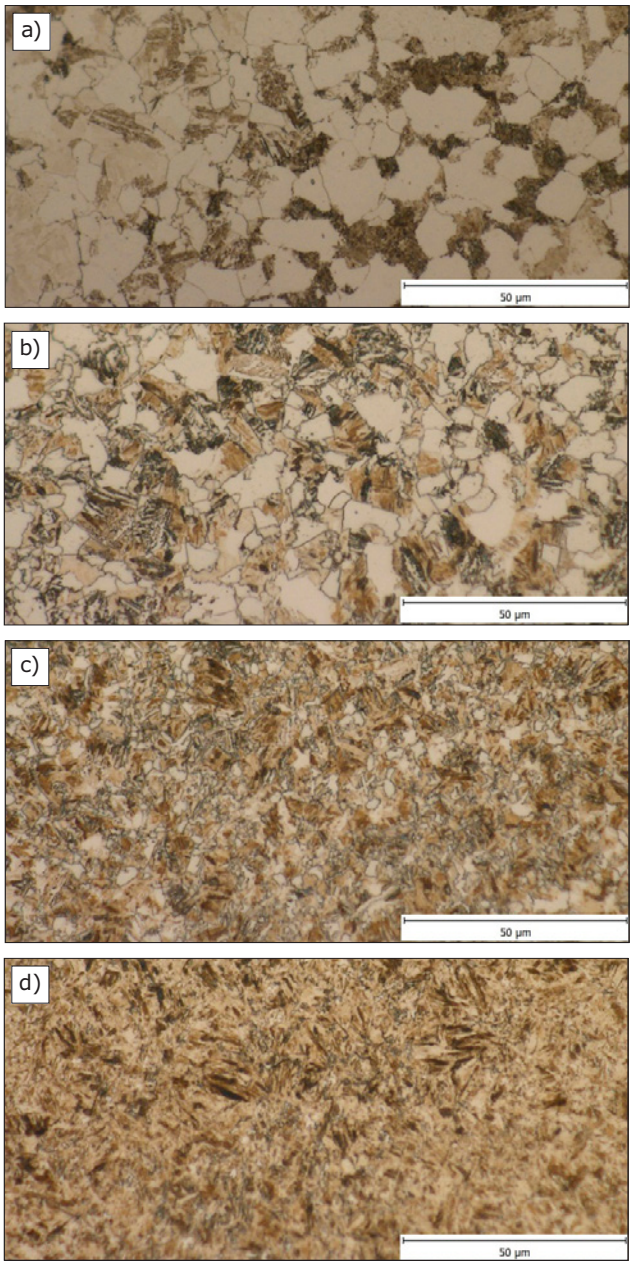

Fig. 10. Selected examples of metallographic analyses of samples from the DCCT diagram ($\dot{e} = 20\ s^{-1}$):
a) 0.2 °C/s = 60 % F + 40 % P
b) 3 °C/s = 50 % F + 35 % P + 10 % B + 5 % M, c) 14 °C/s = 10 % F + 50 % B + 40 % M, d) 50 °C/s = 100 % M (s9)

proportions of individual structural components, are presented in Fig. 10. The analysis results confirmed the relatively high sensitivity of the steel to the formation of quenched structural components at relatively low cooling rates. In cases of common forming practice, the aforementioned situation could be a complicating factor, particularly where the structure should be bainite and martensite-free.

The ratios of individual structural components were determined using image analysis (from optical metallography) and QuickPHOTO INDUSTRIAL software. The comparison of the ratios of the individual structural components in relation to selected and comparable cooling rates is presented in Fig. 11. The diagram reveals that [particularly, at higher cooling rates (above 3 °C/s)] the ratio of diffuse transformation products (F+P) increased because of the previous deformation and at the expense

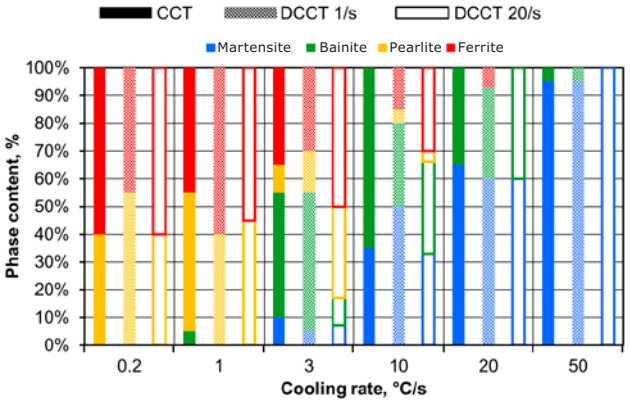

Fig. 11. Comparison of the ratios of individual structural components for selected and comparable cooling rates

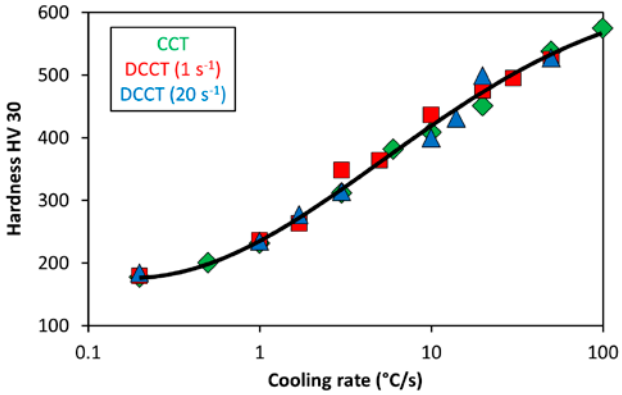

Fig. 12. Comparison of hardness measurements (HV30) in relation to cooling rates and strain rates

of quenched components (B+M). However, the influence of higher strain rates seemed to reduce this effect rather than enhance it.

The results of the dilatometric and metallographic analyses were further supported by the results obtained in hardness measurements (HV30) (see Fig. 12). It was confirmed that hardness increased along with growing proportions of quenched components and, consequently, cooling rates. Regrettably, no significant differences were found as regards measured hardness values (HV30) in relation to all 3 variants of the diagrams.

In order to compare the effect of strain with different strain rates, all three types of diagrams were combined into one comparative (D)CCT diagram (see Fig. 13). This diagram revealed the changes in the transformation regions in relation to specific strain parameters. It could be stated that, in both cases of the strain-affected diagrams, the expected leftward shift of the ferritic and pearlitic regions had taken place, i.e. towards shorter times. Therefore, in both cases it is possible to speak of the acceleration of diffusion transformations triggered by previous deformation. The acceleration itself was induced by an increase in the free enthalpy of austenite triggered by the increasing number of crystallographic lattice defects, whereas the phase transformation of austenite into ferrite tended to heal the lattice defects. Therefore, the decomposition of solidified austenite took place at the higher temperature and in shorter time. At the same time, not only austenite grain boundaries but also deformation bands were sites suitable for ferrite nucleation [1].

Increasing the strain rate to 20 s^{-1} also affected the bainitic transformation, where the area of this transformation was narrowed from nearly all directions (cooling rates and temperature).

In terms of martensite, no significant influence was observed. The only effect of the two variations of strain rates was the shifting of the region of transformation slightly towards higher cooling rates. In terms of the higher cooling rates, the temperature of the start of the martensitic transformation (Ms) appeared to be slightly lower after deformation, yet this could not be predicted with sufficient accuracy and confidence towards the higher cooling rates (above 50 °C/s) based on the tests performed.

However, it was expected that the accelerating effect of ferrite and perlite would be even more pronounced due to the higher strain rate. This, however, was not confirmed. In terms of the pearlitic transformation, only a slight extension of the perlite formation area was observed. As regards the ferritic region, the effect of the higher strain rate translated into the narrowing of the region or the rightward shift of the ferritic nose towards lower cooling rates. However, the comparison of all three diagrams revealed that the curve bounding ferrite formation after the application of a previous strain rate of 20 s^{-1} was located between the curves related to the CCT diagram and the DCCT variant of $\dot{e} = 1\ s^{-1}$. Such a phenomenon could probably be explained by two possible reasons. The first reason could be adiabatic heating (deformation heat), taking place at higher strain rates, usually in excess of 100 s^{-1}. This phenomenon could trigger the coarsening of the austenitic grain. It is known that larger austenitic grains provide fewer nucleation sites suitable for the nucleation of new grains of the same or different structural components. This would then naturally lead to the reduction of the maximum rate at which

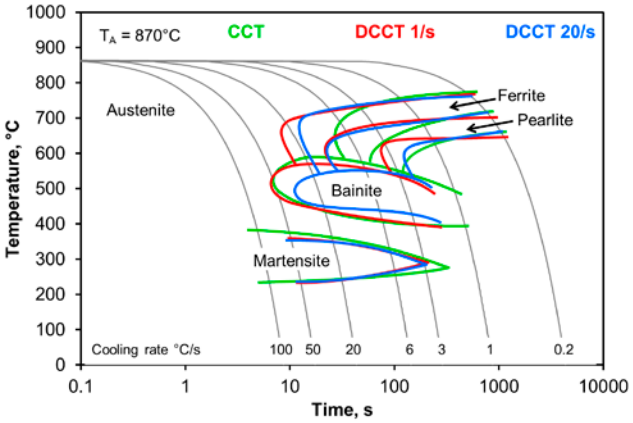

Fig. 13. Comparison (D)CCT diagram of the 25CrMo4 steel

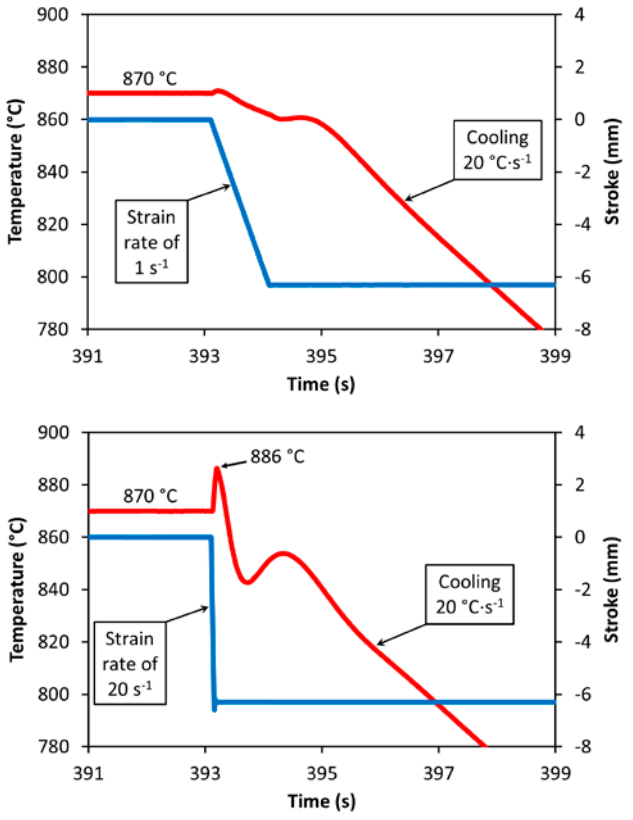

Fig. 14. Examples of temperature control test recordings with the Gleeble plastometer: a) $\dot{e} = 1\ s^{-1}$, b) $\dot{e} = 20\ s^{-1}$

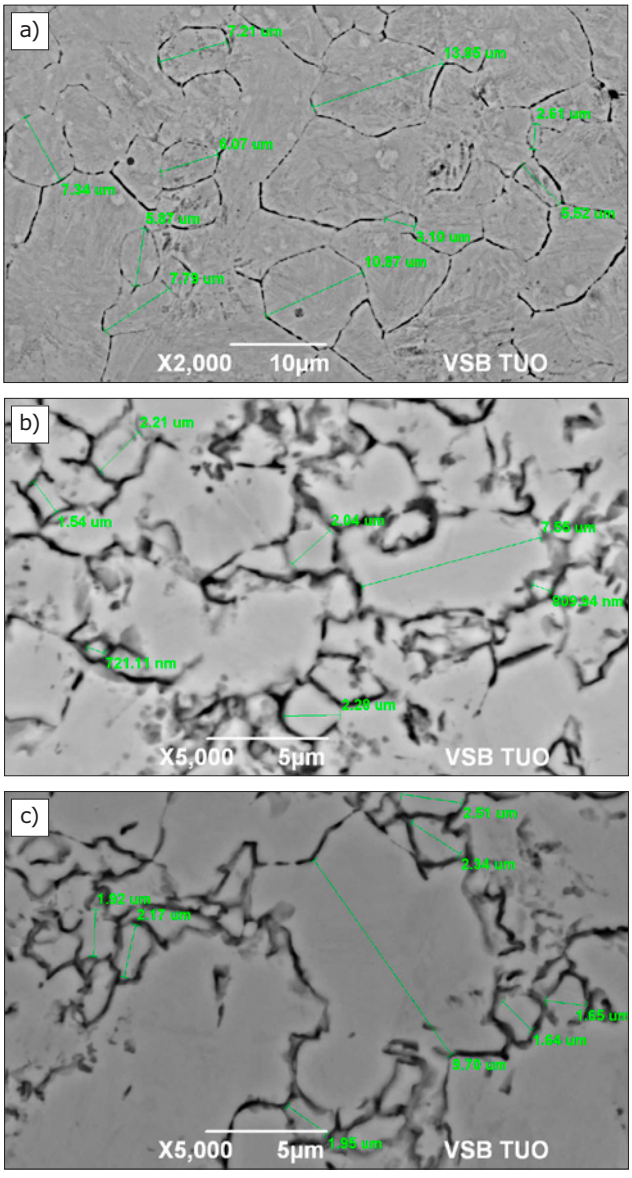

Fig. 15. Analyses (SEM) of specimen structures following the application of the highest cooling rates (preceded by etching of the austenitic grain):
a) without deformation
b) e = 1 s^{-1}
c) $\dot{e} = 20\ s^{-1}$

ferrite formation took place [28, 29]. Despite the fact that the Gleeble system is highly rated because of its precise temperature control, the region directly during and after deformation was investigated in relation to both variations of selected strain rates (Fig. 14). The results confirmed a slight increase in temperature caused by adiabatic heating during strain (particularly in relation to a strain rate of 20 s^{-1}), yet an additional increase of 16 °C within a relatively short time should not result in the noticeable change of the austenite grain size.

The second possible reason explaining the phenomenon of the delay of the ferritic region because of the higher strain rate could be the possible occurrence of grain coarsening, yet not by adiabatic heating, but by incomplete dynamic recrystallization [16]. Since both hypotheses rely on the austenitic grain size, it was necessary to perform SEM-based analyses of sample structures following the application of the highest cooling rates, preceded by the etching of austenitic grain. The results of these analyses are presented in Fig. 15. The crucial point was the comparison of the initial austenitic structure of the samples deformed at various strain rates.

The comparison (Fig. 15) revealed that the initial austenitic grain (in both cases after deformation) was not completely equiaxial and homogeneous in size, i.e. not fully recrystallized. Furthermore, it was also revealed that, in relation to the lower strain rate ($\dot{e}$ = 1 s^{-1}), a larger part of the structure was recrystallized (finer) than that in relation to the higher strain rate ($\dot{e}$ = 20 s^{-1}). As regards the austenitic grain size, there was also no abnormal grain coarsening as the largest grains corresponded in size to the grains without previous strain (about 8–14 μm). It is therefore probable that the higher strain rate delayed the onset of dynamic recrystallisation and, in combination with a selected heating temperature of 870 °C and a selected strain rate of 1, did not lead to the complete recrystallisation of the test steel.

4. Conclusions

Based on the dilatometric tests supported by the metallographic analyses and hardness measurements (HV30), three different (D)CCT transformation diagrams were constructed for 25CrMo4 steel. The diagrams included one CCT diagram and two DCCT diagrams related to the same total deformation value, yet to different strain rates of 1 s^{-1} and 20 s^{-1}. The experiment results justified the formulation of several conclusions.

It was confirmed that test steel 25CrMo4 was strongly sensitive to the formation of quenched structural components (bainite and martensite) over a wide range of cooling rates. Various deformation modes or strain rates did not have a significant effect.

It was also confirmed that, in cases of proeutectoid steels, because of previous deformation, there was the acceleration of diffusion transformations and a slight decrease in temperature limiting the onset of martensitic transformation. The bainitic transformation was only affected by deformation at the higher rate (20 s^{-1}) and in such a way that the entire bainitic region was narrowed, both in terms of temperatures and times.

The comparison involving the effect of the higher (20 s^{-1}) and the lower strain rate (1 s^{-1}) revealed that a strain rate of 20 s^{-1} was responsible for a relatively slight delay at the onset of the formation of primarily ferrite and bainite, whereas other transformations did not have significant influence. The shifts were found to be triggered by the austenitic grain size, particularly by the increased proportion of non-recrystallized coarse grain.

The original assumption of adiabatic (deformation) heat, increasing along with the growing strain rate was refuted. It was documented that this phenomenon did not take place (in relation to relatively precise temperature control in the Gleeble 3800 system). In addition, according to reference publications, adiabatic heat is principally present in steels at strain rates exceeding 100 s^{-1}. As a result, the effect of adiabatic heat was excluded. It was subsequently verified that the phenomenon of delaying the start of ferritic and bainitic transformation was caused by dynamic recrystallization. However, the phenomenon did not take place within the entire volume (which was confirmed by metallographic analyses).

It was finally confirmed that the influence of deformation parameters, i.e. not only the strain rate, could, despite the austenite grain size, affect the kinetics of austenite transformation during continuous cooling through, for example, recrystallization.

REFERENCES

[1] Žídek, M. Metalurgická tvařitelnost ocelí za tepla a za studena. 1. edition. Praha: Aleko, 1995, 348 p.

[2] Kawulok, R., et al. Transformation diagrams of selected steel grades with consideration of deformation effect. Archives of Metallurgy and Materials. 2018, vol. 63, no. 1, pp. 55–60.

[3] Nürnberger, F., et al. Microstructure Transformations in Tempering Steels during Continuous Cooling from Hot Forging Temperatures. Steel Research International. 2010, vol. 81, no. 3, pp. 224–233.

[4] Xu, D. et al. A new study on the growth behavior of austenite grains during heating processes. Scientific Reports. 2017, vol. 7, no. 3968.

[5] Aranda, M., Kim, B., Rementeria, R., et. al. Effect of prior austenite grain size to perlite transformation in a hypereutectoid Fe-C-Mn Steel. Metallurgical and materials transactions A. 2014, vol. 4, pp. 1778–1786.

[6] Farrar, R. A., Zhang, Z., Bannister, S. R., Barritte, G. S. The effect of prior austenite grain size on the transformation behaviour of C-Mn-Ni weld metal. Journal of materials science. 1993, vol. 28, no. 5, pp. 1385–1390.

[7] Kawulok, R., Škandera, D., Kawulok, P., The role of initial structure on transformation kinetics during cooling of steel C10. In: Metal 2017, Conference Proceedings. Ostrava: Tanger Ltd. 2017, pp. 383–389.

[8] Yin, S. B., Sun, X. J., Liu, Q. Y., Zhang, Z. B. Influence of Deformation on Transformation of Low-Carbon and High Nb-Containing Steel During Continuous Cooling. Journal of Iron and Steel Research. 2010, vol. 17, no. 2, pp. 43–47.

[9] Jandová, D., Vadovicová, L. Influence of deformation on austenite decomposition of steel 0.5C-1Cr-0.8Mn-0.3Si, In: Metal 2004, Conference Proceedings. Ostrava: Tanger Ltd. 2004, paper no. 223.

[10] Kruglova, A. A., Orlov, V. V., Khlusova, E. I. Effect of hot plastic deformation in the austenite interval on structure formation in low-alloyed low-carbon steel. Metal Science and Heat Treatment. 2007, vol. 49, no. 11–12, pp. 556–560.

[11] Khlestov, V. M., Konopleva, E. V., Mcqueen, H. J. Effects of deformation and heating temperature on the austenite transformation to pearlite in high alloy tool steels. Materials Science and Technology. 2002, vol. 18, no. 1, pp. 54–60.
[12] Kaspar, R., Lotter, U., Biegus, C. The influence of thermomechanical treatment on the transformation behaviour of steels. Steel Research. 1994, vol. 65, no. 6, pp. 242–247.
[13] Ehl, R., Kruse, M., Oklitz, R., et al. Temperature – controlled rolling of long products – current state of the art. Stahl und Eisen international. 2006, vol. 126, no. 5, pp. S13-S18.
[14] Li, G.Y., Kong, L., Liu, E.Z., Zhang, X.D., Cao, W.Q., Wang, Y.H. Effect of Aging Treatment on the Microstructure and Mechanical Properties of Fe-Mn-Al-C Low Density Steel. IOP Conference Series: Materials Science and Engineering. 2022, vol. 1249, no. 1, pp. 12–53.
[15] Yang, H. S., Bhadeshia, H. K. D. H. Austenite Grain Size and the Martensite–Start Temperature. Scripta Materialia. 2009, vol. 60, no. 7, pp. 493–495.
[16] Schindler, I., Kawulok, R., Opěla, P., Kawulok, P., Rusz, S., Sojka, J., Sauer, M., Navrátil, H., Pindor, L. Effects of Austenitization Temperature and Pre-Deformation on CCT Diagrams of 23MnNiCrMo5-3 Steel. Materials. 2020, vol. 13, paper no. 5116. https://doi.org/10.3390/ma13225116.
[17] Dey, I., Ghosh, S.K., Saha, R. Effects of cooling rate and strain rate on phase transformation, microstructure and mechanical behaviour of thermomechanically processed pearlitic steel. Journal of Materials Research and Technology. 2019, vol. 8, no. 3, pp. 2685–2698, ISSN 2238–7854, https://doi.org/10.1016/j.jmrt.2019.04.006.
[18] Mohamadizadeh, A., Zarei-Hanzaki, A., Heshmati-Manesh, S., Imandoust, A. The effect of strain induced ferrite transformation on the microstructural evolutions and mechanical properties of a TRIP-assisted steel. Materials Science and Engineering: A. 2014, vol. 607, pp. 621–629, ISSN 0921-5093, https://doi.org/10.1016/j.msea.2014.04.044.
[19] Sahu, P., Curtze, S., Das, A., Mahato, B., Kuokkala, V.-T., & Chowdhury, S.G. Stability of austenite and quasi-adiabatic heating during high-strain-rate deformation of twinning-induced plasticity steels. Scripta Materialia. 2010, vol. 62, no. 1, pp. 5–8. https://doi.org/10.1016/j.scriptamat.2009.09.010.
[20] Talonen, J., Hänninen, H., Nenonen, P. et al. Effect of strain rate on the strain-induced γ → α′-martensite transformation and mechanical properties of austenitic stainless steels. Metall Mater Trans A. 2005, vol. 36, pp. 421–432. https://doi.org/10.1007/s11661-005-0313-y.
[21] Kawulok, R., Schindler, I., Sojka, J., Kawulok, P., Opěla, P., Pindor, L., Grycz, E., Rusz, S., Ševčák, V. Effect of Strain on Transformation Diagrams of 100Cr6 Steel. Crystals. 2020, vol. 10, paper no. 326. https://doi.org/10.3390/cryst10040326.
[22] Grajcar, A., Kuziak, R., Zalecki, W. Designing of cooling conditions for Si-Al microalloyed TRIP steel on the basis of DCCT diagrams. J. Achiev. Mater. Manuf. Eng. 2011, vol. 45, pp. 115–124.
[23] Pohjonen, A., Somani, M., Porter, D. Effects of Chemical Composition and Austenite Deformation on the Onset of Ferrite Formation for Arbitrary Cooling Paths. Metals. 2018, vol. 8, paper no. 540. https://doi.org/10.3390/met8070540.
[24] Kantanen, P. K., Javaheri, V., Somani, M. C., Porter, D. A., Kömi, J. I. Effect of deformation and grain size on 5titioning of (high) silicon-aluminum steels. Materials Characterization. 2021, vol. 171, paper no. 110793, ISSN 1044-5803, https://doi.org/10.1016/j.matchar.2020.110793.
[25] Abbasi, M., Saeed-Akbari, A., Naderi, M. The effect of strain rate and deformation temperature on the characteristics of isothermally hot compressed boron-alloyed steel. Materials Science and Engineering: A. 2012, vol. 538, pp. 356–363, ISSN 0921-5093, https://doi.org/10.1016/j.msea.2012.01.060.
[26] Dynamic Systems Inc. 39112 Non-contact scanning optical system user's manual. Poestenkill, NY: DSI, 2015, 28 p.
[27] Kawulok, P., et al. Výzkum deformačního chování a modelování procesů objemového tváření na simulátoru HDS-20. In: 81. seminar OCELOVÉ PÁSY – Možnosti studia deformačního chování materiálu a fyzikálních simulací procesů válcování na FMMI VŠB-TUO, Conference Proceedings. Ostrava, 2018, pp. 45–95. ISBN 978-80-248-4173-1.
[28] Bharadwaj, R., Sarkar, A. & Rakshe, B. Effect of Cooling Rate on Phase Transformation Kinetics and Microstructure of Nb–Ti Microalloyed Low Carbon HSLA Steel. Metallogr. Microstruct. Anal. 2022, vol. 11, pp. 661–672. https://doi.org/10.1007/s13632-022-00864-9.
[29] Chen, R. C., Hong, C., Li, J. J., Zheng, Z. Z., Li, P. C. Austenite grain growth and grain size distribution in isothermal heat-treatment of 300M steel. Procedia Engineering. 2017, vol. 207, pp. 663–668, ISSN 1877-7058, https://doi.org/10.1016/j.proeng.2017.10.1038.